JACS
JOURNAL OF THE AMERICAN CHEMICAL SOCIETY

COMMUNICATION

pubs.acs.org/JACS

Hydrogen-Incorporation Stabilization of Metallic VO_2(R) Phase to Room Temperature, Displaying Promising Low-Temperature Thermoelectric Effect

Changzheng Wu,[†] Feng Feng,[†] Jun Feng,[†] Jun Dai,[†] Lele Peng,[†] Jiyin Zhao,[†] Jinlong Yang,[†] Cheng Si,[‡] Ziyu Wu,[‡] and Yi Xie*[,†]

[†]Hefei National Laboratory for Physical Sciences at Microscale and [‡]National Synchrotron Radiation Laboratory, University of Science & Technology of China, Hefei, Anhui 230026, P.R. China

Supporting Information

ABSTRACT: Regulation of electron−electron correlation has been found to be a new effective way to selectively control carrier concentration, which is a crucial step toward improving thermoelectric properties. The pure electronic behavior successfully stabilized the nonambient metallic VO_2(R) to room temperature, giving excellent thermoelectric performance among the simple oxides with wider working temperature ranges.

Thermoelectric effects realize the direct conversion from thermal to electrical energy, presenting promising signs for direct conversion of waste heat to electric power that is vital for energy harvesting and conversion.[1−3] Superior thermoelectric materials rely on simultaneously achieving high electrical conductivity (σ), high thermoelectric power (S), and low thermal conductivity (κ). There is a strong correlation of these three parameters according to the Wiedemann−Franz law,[4] which explains the practical difficulty in effectively enhancing thermoelectric performance during the past decades. All the three parameters are highly dependent on the details of the electronic structure and the charge carrier-related properties.[5,6]

Strongly correlated electronic systems give a new intriguing platform for regulating carrier concentration. For correlated systems, active control and manipulation of the charge and spin degrees of freedom of the electrons as well as the atomic orbital orientations would create the expected electronic structure and charge carrier-related properties. Monoclinic VO_2(M) is the prototype material for interpreting correlation effects in solids,[7] in which the relationship between the correlated effects and electronic structure has been extensively pursued. As is known, monoclinic VO_2(M) (room-temperature phase, <340 K) and rutile VO_2(R) (nonambient phase, >340 K) are typical states in a temperature-driven, fully reversible structural phase-transition process. The position shifting of vanadium atoms from zigzag-type in VO_2(M) to linear chains in VO_2(R) brings about the evolution from localized d-orbital electron cloud to delocalized state along the c-axis direction.[8,9] In this regard, the orientation change of the electron clouds influences the state of electron spin on passing through the phase transition, resulting in the widening/narrowing of the material bandgap to form insulator or metal states for monoclinic VO_2(M) and rutile VO_2(R); this reveals an intriguing route to control the carrier concentration by modulating related effects of electronic properties.[10] Of note, systematic investigation of thermoelectric effects of vanadium oxides has been long neglected. For vanadium oxides, heavy-ion doping, e.g., using W^{6+} and Mo^{6+} ions, is usually regarded as the classic way to control the carrier concentrations. In effect, traditional doping with higher valence ions (W^{6+} and Mo^{6+}) could increase the carrier concentration due to the enhancement of the electron concentration from doping.[11,12] However, the heavy heterogeneous ions involved in a M-doped VO_2(M) (M = W^{6+} and Mo^{6+}) crystal lattice would inevitably complicate the thermoelectric material systems: (i) the added atomic species of doping ions complicates the influence on thermoelectric properties, especially for electrical conductivity and thermoconductivity; (ii) the doped ions inevitably cause structural distortion in the doped compounds accompanying the injection of additional electrons into the V−O frameworks. These two entangled structural change and electron−electron effects hinder the construction of an effective model to investigate the influence of electron−electron correlation effects on thermoelectric performance.

Herein we highlight a new pathway to successfully modulate the strong correlation effects in vanadium dioxides. The carrier concentrations can be effectively controlled only by the injection of additional electrons into rutile V−O frameworks. Exterior modification using the lightest hydrogen atoms, without changing the V−O framework of rutile VO_2(R), successfully stabilizes nonambient metallic VO_2(R) phase at room temperature, with the lightest H^+ ions contributing the additional electrons into the infinite V^{4+}−V^{4+} chains and thus enhancing the electron−electron correlation effects in rutile structure. By controlling the hydrogen concentrations, metallic rutile VO_2(R), semiconducting monoclinic VO_2(M), and their intermediate states, the mixture of metallic VO_2(R) and semiconducting VO_2(M) (VO_2-(M-R)) polymorphs, are all achieved at room temperature with carrier concentration gradients, giving an ideal model to investigate thermoelectric effects.

Heating the as-prepared black hydric paramontroseite VO_2 in a N_2 gas flow at 250, 300, and 600 °C produces the vanadium oxides with gradient hydrogen contents of 3.8‰, 1.3‰, and approaching zero (Supporting Information (SI), section S1),

Received: April 7, 2011
Published: June 02, 2011

ACS Publications © 2011 American Chemical Society

dx.doi.org/10.1021/ja203186f | *J. Am. Chem. Soc.* 2011, 133, 13798–13801

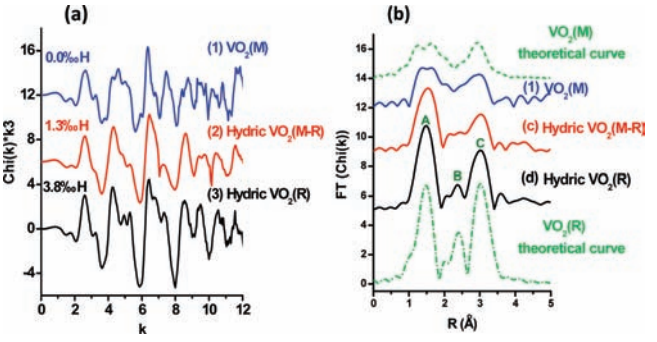

Figure 1. V K-edge EXAFS oscillations $[\chi(\kappa)]$ (a) and their Fourier transforms (b) at room temperature for the as-obtained hydric vanadium dioxide samples.

which could be indexed to hydric rutile VO_2(R), hydric VO_2-(M-R), and monoclinic VO_2(M) at room temperature, respectively, according to systematic characterizations. The XRD patterns provide direct structural information on the as-obtained vanadium oxides. The sample with 3.8‰ hydrogen concentration has the typical XRD features of rutile VO_2 structure: (i) the absence of the typical XRD peaks $(100)_M$ (26.94°) and $(-102)_M$ (33.40°) (Figure S3); (ii) the shifting of VO_2(R) (110) peak to lower 2θ compared with VO_2(M) (011) peaks at $26° \le 2\theta \le 29°$ (Figure S3d); (iii) the splitting of VO_2(R) (310) and (002) in $64° \le 2\theta \le 66°$ evolved from VO_2(M) (130) peak (Figure S3e). The sample with 3.8‰ hydrogen (Figure S3a) can be readily indexed to tetragonal rutile VO_2(R) (JCPDS Card No. 79-1655, a = 4.552 Å, c = 2.856 Å), indicating that hydrogen incorporation stabilizes nonambient rutile VO_2(R) phase to room temperature. The sample without hydrogen (Figure S3c) was characterized as monoclinic VO_2(M) (JCPDS Card No. 82-0661, a = 5.751 Å, b = 4.528 Å, c = 5.380 Å), while the sample with 1.3‰ hydrogen was indexed to the intermediate states between rutile and monoclinic phases, named hydric VO_2(M-R). The room-temperature metallic rutile VO_2(R) is also verified by the HRTEM result (SI, section S3).

Synchrotron radiation XAFS further revealed the local structural information of the samples. Figure 1 shows V K-edge XAFS spectra at room temperature. The extended XAFS (EXAFS) functions $\chi(k)$ and Fourier transforms exhibit remarkable differences among the three samples, with the typical features of rutile VO_2(R), intermediate VO_2(M-R) states, and monoclinic VO_2(M), respectively. The $\chi(k)$ oscillation shape of monoclinic VO_2(M) is significantly different from that of rutile VO_2(R), at 4−8 $Å^{-1}$ (Figure 1a), and the Fourier transform profiles in real space clearly give direct evidence for the room-temperature rutile VO_2(R). As is known, there are four distinct peaks for characterizing monoclinic VO_2(M), those for the V−O split (1.20 and 1.63 Å) and V−V bonds (V−V1 2.12 Å and V−V2 2.88 Å) (SI, section S4), while for rutile structure, due to the increased structural symmetry of rutile lattices, the two V−O split peaks (1.20 and 1.63 Å) in monoclinic VO_2(M) usually merge into one single peak at 1.48 Å in VO_2(R), as shown in Figure 1b.[13] Also, since the neighboring V−V bond length of 2.88 Å for the infinite linear V−V chains along the VO_2(R) c-axis is larger than that of V−V dimerization (2.65 Å) in VO_2(M) (SI, section S4), the V−V1 peak at 2.12 Å in VO_2(M) shifts to 2.36 Å for rutile structure.[14] The curve features of VO_2 samples with 3.8‰ and nearly zero hydrogen concentrations are in good agreement with those calculated from the theoretical rutile and monoclinic VO_2 structures, respectively.

FTIR and Raman spectra (SI, section S5) further reveal structural and electrical information about VO_2(M) and VO_2(R). The depressed fingerprint peaks[15−17] in the FTIR and Raman spectra verified the presence of metallic VO_2(R) at room temperature due to the higher structural symmetry of rutile VO_2 (*P42/mmm*, No. 136). The systematic characterizations clearly verified the realization of metallic VO_2(R) at room temperature.

The hydrogen concentrations of the VO_2 samples were determined by elemental analysis and by FTIR and ^{1}H solid-state MAS NMR spectra. Based on the calculation results of the bulk elemental analysis by a VARIO ELIII (German) element analytical instrument (SI, section S6), the hydrogen contents of hydric rutile VO_2(R), hydric VO_2(M-R), and monoclinic VO_2-(M) are 3.8‰, 1.3‰, and about zero, respectively. These results were further verified by peak intensities of O−H deformation vibrations in FTIR (Figure S7) and ^{1}H solid-state MAS NMR (Figure S9) spectra for samples with the same H content.

As described above, with the hydrogen incorporation into the rutile structure, the nonambient rutile phase existed at ambient conditions. Due to the unchanged vanadium−oxygen lattice framework, as evidenced by the above structural characterizations, the hydrogen ions could only incorporate into the exterior environments, such as the 1×1 tunnels or crystal surface of rutile crystal, ensuring no structural distortions of the main lattice framework. In effect, the incorporation of H^+ ions in the exterior locations contributes additional electrons to the V−O systems, the effect of which is similar to that of heavy ions (such as W^{6+}, Mo^{6+}) doping.[11,12] The extra electrons in the V−O system would enhance the electron−electron correlation effects between the neighboring vanadium atoms in the infinite linear V−V chains. To confirm that H^+ incorporation indeed enhances the electron correlation, we performed density functional theory calculations based on the experimental atomic structural parameters. As shown in Figure 2a, we plot the partial density of states (DOS) of the d_{z^2} orbital of vanadium in hydric VO_2(R). The d_{z^2} orbital should receive more attention due to the linear orbit clouds extending along the z-direction, which is the direction of the infinite V−V chains in rutile structure. The sharing of d_{z^2} electrons by all of the vanadium atoms in the infinite V−V chain produces the electron−electron correlation effects, the localization/delocalization of which determines the electronic states. For the calculated results, in pure rutile phase without H^+ incorporation, this orbital is an unoccupied one, while upon H^+ incorporation, the DOS of d_{z^2} shows some peaks just below the Fermi level, which means bonding between d_{z^2} orbitals of nearest-neighboring vanadium atoms and enhanced electron−electron correlation effects along the infinite linear V−V chains. In effect, the enhanced correlation effects strengthen the correlation effects of infinite V−V chains in rutile VO_2, which are hard to break even when temperature is decreased, and thus stabilize the metallic VO_2(R) down to room temperature.

DSC curves (Figure S10) showing the phase-transition behavior indicate the material state at a given temperature.[10] Moreover, ZFC magnetization curves (Figure S11) also reveal phase-transition behaviors consistent with DSC results. As a summary, Figure 2b illustrates the evolution of the phase-transition temperature with hydrogen concentration, revealing that around room temperature (25 °C), the samples with 1.3‰ and no H incorporation are the intermediate coexisting rutile and monoclinic states, respectively, while the sample with 3.8‰ H is the metallic rutile VO_2(R) phase.

dx.doi.org/10.1021/ja203186f |*J. Am. Chem. Soc.* 2011, 133, 13798–13801

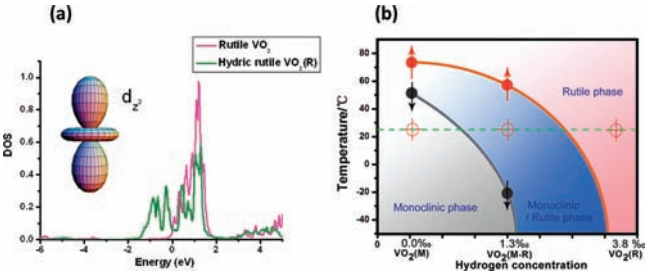

Figure 2. (a) Partial density of states (DOS) of d_{z^2} orbital of vanadium of the hydric VO_2(R); inset is the d_{z^2} orbital. (b) Evolution of the transition temperature, T_c, with change in hydrogen concentration. Red traces indicate the rutile → monoclinic phase-transition temperatures, $T_c\uparrow$, on heating; the black traces indicate the monoclinic → rutile phase-transition temperatures, $T_c\downarrow$, on cooling.

The temperature-dependent resistivity curves also well reflect the typical phase-transition behavior. As shown in Figure 3a, for monoclinic VO_2(M) sample, a pronounced one-order drop in resistivity with temperature increase to near 340 K clearly shows the typical electrical transition originating from the slight atom shifting during the structural transition. The hydric VO_2(M-R) sample has an elongated decreasing transition period with increasing temperature, as shown in Figure 3b, indicating it has a very broad electrical resistivity transition range. However, the hydric VO_2(R) has no obvious resistivity changes in the concerned temperature range, and the electrical resistivity only slightly increases with increasing temperature (Figure 3c), consistent with metal behavior. Hall measurement results reveal that the hydric VO_2(R), hydric VO_2(R-M), and monoclinic VO_2(M) samples have carrier concentrations of 5.04×10^{19}, 9.44×10^{17}, and 2.30×10^{16}, respectively, at ambient temperature. It is understandable that the metallic VO_2(R) has the largest carrier concentration, and the semiconducting VO_2(M) has the lowest.

The hydrogen incorporation into rutile structure successfully realized metallic hydric rutile VO_2(R), the intermediate VO_2(M-R) state, and semiconducting monoclinic VO_2(M), giving the gradient carrier concentrations at room temperature. The corresponding thermoelectric characterization shows that they are all n-type with negative Seebeck coefficient S (thermopower).[18] As the hydrogen concentration increases from near zero (monoclinic VO_2(M)), to 1.3‰ (hydric VO_2(R-M)), to 3.8‰ (hydric VO_2(R)), the maximum thermopower S_{max} decreases from −136.4, to −87.7, to −55.1 μV/K, respectively. That is to say, the monoclinic VO_2(M) has a superior Seebeck coefficient than hydric VO_2(R), which is understandable based on the hybrid density functional calculation results near the Fermi surface. As is shown in Figure S12, the DOS of monoclinic VO_2(M) varies rapidly near E_f, and that of hydric VO_2(R) does not. Based on the Mott formula,[19]

$$S = \frac{\pi^2}{3}\frac{k^2 T}{e}\frac{\mathrm{d}\ln\sigma(E)}{\mathrm{d}E}\bigg|_{E=E_f}$$

the thermopower S_{max} is proportional to the logarithmic derivative of $\sigma(E)$ with respect to E near the Fermi level. The monoclinic VO_2(M) with rapidly changing DOS near the Fermi level is expected to have a larger thermopower S_{max} than hydric VO_2(R). Moreover, the temperature of S_{max} is strongly dependent on the bandgap size of the as-obtained VO_2 samples. For semiconducting VO_2(M), the observed temperature of maximum S is 318 K, while

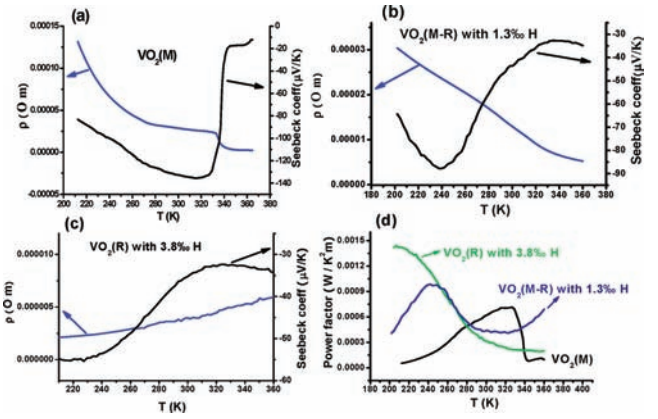

Figure 3. Temperature dependence of the electrical resistivity ρ (Ω) and the Seebeck coefficient S (μV/K) for monoclinic VO_2(M) with hydrogen content 0‰ (a), hydric VO_2(M-R) with hydrogen content 1.3‰ (b), and hydric VO_2(R) with hydrogen content 3.8‰ (c). The resistivity and thermopower measurements were performed on samples of typical size $8 \times 6 \times 3$ mm^3. (d) Temperature dependence of the power factor PF = σS^2 for monoclinic VO_2(M), hydric VO_2(M-R), and hydric VO_2(R).

for metallic hydric VO_2(R) with zero bandgap, it is 220 K, as shown in Figure 3. In effect, the wider bandgap would delay the onset of extra carrier excitation from the valence to the conduction bands that was responsible for higher thermopower, and then S_{max} is attained at higher temperatures.[20] Thus, the wider bandgap of semiconducting VO_2(M) resulted in the higher temperature of S_{max}, while the temperature of S_{max} for the zero bandgap hydric VO_2 is 220 K. By regulating the correlation effects via hydrogen incorporation, the observed temperatures for maximum thermopower are well-controlled in a wide temperature range from 220 to 318 K.

Atomic weight and structural symmetry were responsible for the thermal conductivity. Usually, heavy atoms give rise to low acoustic phonon frequency, and the low structural symmetry generates the long and tortuous mean free paths; both lead to high thermal resistance.[21,22] Our three VO_2 samples had the same atom compositions, and the relatively lighter atomic weight of vanadium (55.847 g/mol) resulted in relatively higher thermal conductivity from 2.2 to 4.0 W/mK, compared with conventional thermoelectric materials (usually 0.5−1 W/mK).[21,22] Also, due to the higher structural symmetry of rutile than monoclinic structure, the thermal conductivity of hydric rutile VO_2(R) is higher than that of monoclinic VO_2(M) (Figure 4a).

In Figure 4b, the figures of merit for vanadium dioxide samples, calculated from the above data with the relationship $ZT = S^2T/\rho\kappa$, are summarized. For hydric VO_2(R), at 210.0 K, the figure of merit reaches the maximum value of 0.12; for hydric VO_2(R-M), ZT_{max} = 0.089 at 240.4 K, and for VO_2(M), ZT_{max} = 0.071 at 316.6 K. Here, the temperature of ZT_{max} decreases from 316.6, to 240.4, to 210.0 K, with the narrowing bandgap from semiconducting VO_2(M), to hydric VO_2(M-R) state, to metallic hydric VO_2(R), respectively, which is reminiscent of the features of the temperature-dependent power factor curve (Figure 3d). Our figure of merit behavior confirms the ability to achieve the thermoelectric devices with a wide range of working temperature. Of note, the hydric VO_2(R) achieves a high ZT_{max} = 0.12 at the low temperature of 210.0 K, which is higher than those for hydric VO_2(R-M) (0.089, 240.4 K) and monoclinic VO_2(M) (0.071, 316.6 K). The key reason why room-temperature hydric VO_2(R)

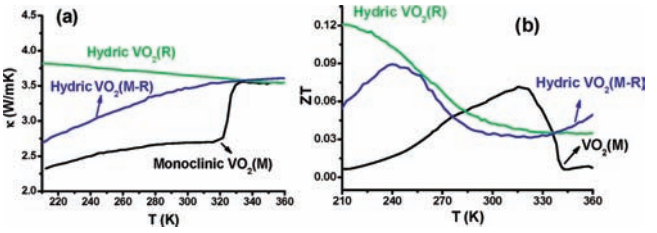

Figure 4. (a) Temperature dependence of the thermal conductivity κ of monoclinic VO_2(M) with absence of H, hydric VO_2(M-R) with hydrogen content of 1.3‰, and hydric VO_2(R) with hydrogen content of 3.8‰. (b) Temperature dependence of the thermoelectric figure of merit ZT for monoclinic VO_2(M), hydric VO_2(M-R), and hydric VO_2(R).

exhibits such good thermoelectric properties is its high electric conductivity, resulting from the incorporation of hydrogen atoms into the rutile structure. The residual incorporated H^+ in rutile structure would contribute more electrons to rutile vanadium oxide frameworks, leading to stronger electron−electron correlation effects between the nearest-neighboring V−V chains. The enhanced correlation effects effectively increase the carrier concentrations and result in good thermoelectric properties.

In conclusion, we successfully modulated the electron−electron correlation effects in rutile VO_2(R) by a novel pathway with the lightest atom (H^+) incorporation into rutile structure. The injection of additional electrons into the vanadium−oxygen lattice frameworks successfully stabilized the nonambient rutile VO_2(R) phase to room temperature. Also, we describe a new physical scenario in which regulation of electron−electron correlation is an effective model for selectively controlling the metallic and semiconducting states, giving larger than 3 orders of magnitude carrier concentrations gradients, which leads to the improved thermoelectric performance in a wide working temperature range, especially in near or below room temperature. Of note, very few simple oxides are known that can achieve a high ZT value below room temperature.[20] Our findings reveal that regulating the electron−electron correlation effects in solids allows advances in controlling carrier concentrations, with promising signs for designing new thermoelectric materials via active control of electronic structures and charge carrier-related properties.

■ ASSOCIATED CONTENT

Supporting Information. Experimental and characterization details and calculated DOS. This material is available free of charge via the Internet at http://pubs.acs.org.

■ AUTHOR INFORMATION

Corresponding Author
yxie@ustc.edu.cn

■ ACKNOWLEDGMENT

This work was financially supported by National Basic Research Program of China (No. 2009CB939901), NSFC (Grant No.11074229, 10979047, 20801051, 90922016, 11079004), program for New Century Excellent Talents in University, Fundamental Research Funds for the Central Universities, and CAS project KJCX2-YW-H2O.

■ REFERENCES

(1) Heremans, J. P.; Jovovic, V.; Toberer, E. S.; Saramat, A.; Kurosaki, K.; Charoenphakdee, A.; Yamanaka, S.; Snyder, G. J. *Science* **2008**, *321*, 554.
(2) Johnsen, S.; He, J. Q.; Androulakis, J.; Dravid, V. P.; Todorov, I.; Chung, D. Y.; Kanatzidis, M. G. *J. Am. Chem. Soc.* **2011**, *133*, 3460.
(3) Yu, J.-K.; Mitrovic, S.; Tham, D.; Varghese, J.; Heath, J. R. *Nat. Nanotech.* **2010**, *5*, 718.
(4) Kanatzidis, M. G. In *Semiconductors and Semimetals*; Terry, M. T., Ed.; Elsevier: Amsterdam, 2001; Vol. 69, p 51.
(5) Ye, X. C.; Chen, J.; Murray, C. B. *J. Am. Chem. Soc.* **2011**, *133*, 2613.
(6) Zhao, Y.; Dyck, J. S.; Hernandez, B. M.; Burda, C. *J. Am. Chem. Soc.* **2010**, *132*, 4982.
(7) Cavalleri, A. *Science* **2007**, *318*, 755.
(8) Grinolds, M. S.; Lobastov, V. A.; Weissenrieder, J.; Zewail, A. H. *Proc. Natl. Acad. Sci. U.S.A.* **2006**, *103*, 18427.
(9) Wu, C. Z.; Dai, J.; Zhang, X.-D.; Yang, J.-L.; Qi, F.; Gao, C.; Xie, Y. *Angew. Chem., Int. Ed.* **2010**, *49*, 4.
(10) Berglund, C. N.; Guggenheim, H. J. *Phys. Rev.* **1969**, *185*, 1022.
(11) Goodenough, J. B.; Hong, H. Y. P. *Phys. Rev. B* **1973**, *8*, 1323.
(12) Mitsumata, T.; Sakai, K.; Takimoto, J.-i. *J. Phys. Chem. B* **2006**, *110*, 20217.
(13) Booth, J. M.; Casey, P. S. *Phys. Rev. Lett.* **2009**, *103*, 086402.
(14) Yao, T.; Zhang, X.; Sun, Z.; Liu, S.; Huang, Y.; Xie, Y.; Wu, C.; Yuan, X.; Zhang, W.; Wu, Z.; Pan, G.; Hu, F.; Wu, L.; Liu, Q.; Wei, S. *Phys. Rev. Lett.* **2010**, *105*, 226405.
(15) Wu, C.-Z.; Zhang, X.-D.; Dai, J.; Yang, J.-L.; Wu, Z.-Y.; Wei, S.-Q.; Xie, Y. *J. Mater. Chem.* **2011**, *21*, 4509.
(16) Valmalette, J. C.; Gavarri, J. R. *Mater Sci. Eng. B* **1998**, *54*, 168.
(17) Chou, J. Y.; Lensch-Falk, J. L.; Hemesath, E. R.; Lauhon, L. J. *J. Appl. Phys.* **2009**, *105*, 0343101–6.
(18) Qiu, X.; Austin, L. N.; Muscarella, P. A.; Dyck, J. S.; Burda, C. *Angew. Chem., Int. Ed.* **2006**, *45*, 5656.
(19) *The Theory of the Properties of Metals and Alloys*; Mott, N. F., Jones, H., Eds.; Dover Publications: New York, 1958.
(20) Chung, D.-Y.; Hogan, T. P.; Rocci-Lane, M.; Brazis, P.; Ireland, J. R.; Kannewurf, C. R.; Bastea, M.; Uher, C.; Kanatzidis, M. G. *J. Am. Chem. Soc.* **2004**, *126*, 6414.
(21) Zhang, G.; Wang, W.; Li, X. *Adv. Mater.* **2008**, *20*, 3654.
(22) Zhou, M.; Li, J.-F.; Kita, T. *J. Am. Chem. Soc.* **2008**, *130*, 4527.